

**Ba isotopic signature for early differentiation between Cs and Ba  
in natural fission reactors**

**Hiroshi Hidaka<sup>1,2,3\*</sup> and François Gauthier-Lafaye<sup>3</sup>**

<sup>1</sup>*Department of Earth and Planetary Systems Science, Hiroshima University  
Higashi-Hiroshima 739-8526, JAPAN*

<sup>2</sup>*Project Center of Multi-Isotope Research for Astro- & Geochemical Evolution  
(MIRAGE), Higashi-Hiroshima 739-8526, JAPAN*

<sup>3</sup>*Centre de Geochimie de la Surface, Ecole et Observatoire des Sciences de la Terre,  
UMR7517-CNRS-ULP, 1 rue Blessig, 67084 Strasbourg, FRANCE*

\*corresponding author

## **Abstract**

Ba isotopic studies of the Oklo and Bangombe natural fission reactors in east Gabon provide information on the geochemical behavior of radioactive Cs ( $^{135}\text{Cs}$  and  $^{137}\text{Cs}$ ) in a geological medium. Large isotopic deviations derived from fissionogenic Ba were found in chemical leachates of the reactor uraninites. The fissionogenic Ba isotopic patterns calculated by subtracting the non-fissionogenic component are classified into three types that show different magnifications of chemical fractionation between Cs and Ba. In addition, the isotopic signatures of fissionogenic  $^{135}\text{Ba}$ ,  $^{137}\text{Ba}$  and  $^{138}\text{Ba}$  suggest an early differentiation between Cs and Ba of less than 20 years after the production of fissionogenic Cs and Ba. On the other hand, only small excesses of  $^{135}\text{Ba}$  ( $\epsilon < +1.8$ ) and/or  $^{137}\text{Ba}$  ( $\epsilon < +1.3$ ) were identified in some clay samples, which might have resulted from selective adsorption of  $^{135}\text{Cs}$  and  $^{137}\text{Cs}$  that migrated from the reactors by differentiation.

## 1. INTRODUCTION

The Oklo, Okelobondo, and Bangombé uranium deposits in the Republic of Gabon, central Africa, are well known as natural fission reactors, because large-scale spontaneous fission reactions occurred in some parts of the deposits, which we call “reactor zones (hereafter, RZs)”. Geochemical studies of the RZs can be used to understand the long-term behaviors of many fission products generated in the reactors. In particular, isotopic measurements using several mass spectrometric techniques are effectively used to trace fission products in and around the RZs (DeLaeter and Hidaka, 2007).

Since the yield of radioactive Cs is high in a spent nuclear fuel, understanding the long-term behavior of Cs in environments is important for the disposal of radioactive waste. Because Cs ( $^{133}\text{Cs}$ ) is a mono-isotopic element, fissionogenic and non-fissionogenic  $^{133}\text{Cs}$  cannot be directly distinguished by mass spectrometric techniques. However, isotopic abundance patterns of fissionogenic Ba in the RZs provide useful information on the geochemical behavior of long-lived  $^{135}\text{Cs}$  ( $t_{1/2}=2.3$  Ma) and  $^{137}\text{Cs}$  ( $t_{1/2}=30$  a) that ultimately decay to  $^{135}\text{Ba}$  and  $^{137}\text{Ba}$ , respectively. Figure 1 indicates a part of the nuclear chart around Ba showing the fissionogenic and radioactive decay characteristics including the Cs-Ba system. Barium has seven stable isotopes with the mass numbers 130, 132, 134, 135, 136, 137 and 138. Among seven isotopes,  $^{135}\text{Ba}$ ,  $^{137}\text{Ba}$  and  $^{138}\text{Ba}$  are produced by fission. Previous studies showed that long-lived fissionogenic Cs isotopes as well as Rb, Sr and Ba were almost completely removed from the reactors because of their incompatibilities with the  $\text{UO}_2$  crystalline structure, and their high solubility and reactivity (Brookins et al., 1975; Hidaka et al., 1992). However, small but significant amounts of these elements remained in the core of RZ10, which is well protected from weathering because of its deep location (Hidaka et al., 1993; Hidaka and Holliger, 1998).

It is calculated that more than 90 % of fissionogenic Cs was removed even in less weathered RZs (Hidaka et al., 1993). Our major concern is where most of the fissionogenic Cs has gone. It has been known, through the microscopic observation of artificial spent fuel, that fissionogenic Cs and Ba migrate to grain boundaries and fractures between the edge of the fuel pellet and the surrounding metal cladding, and form oxide precipitates (Kleykamp, 1985). In this study, precise Ba isotopic measurements of not only RZ uraninite but also clay minerals from the peripheral rocks of the Oklo and

Bangombé RZs were performed, because clay minerals are generally known to adsorb Cs well. There are many studies particularly on the adsorption behavior of Cs on clay minerals (e.g., Sawhney, 1970; Commans and Hockley, 1992; Poinssot et al., 1999; Vejsada et al., 2005).

On the other hand, microscale isotopic analysis by secondary ion mass spectrometry (SIMS) provides information on the selective uptake of fissionogenic isotopes into specific minerals (Horie et al., 2004; Hidaka et al., 2005; Kikuchi et al., 2007). In particular,  $^{206}\text{Pb}$  isotopic excesses of illite in the surrounding rocks of RZ are concluded as a result of the adsorption of  $^{226}\text{Ra}$  leached out of the RZ uraninite (Hidaka et al., 2007). The illite grains studied for the Pb isotopic measurements also included large amounts of Ba (1230 to 6010 ppm), suggesting the selective adsorption of Ba together with Ra onto the illite grains. Unfortunately we could not confirm the existence of fissionogenic Ba in the illite from the isotopic data using SIMS because of the low analytical precision. Prior to the isotopic measurements, thin section samples were prepared and observed using an electron probe microanalyzer (EPMA) to find any Cs aggregate materials. Although we expected Cs-Ba oxide aggregates in the peripheral rocks of the natural reactors, visible Cs-Ba aggregates could not be identified from our preliminary EPMA observation.

The first aim of this study is to identify the existence of fissionogenic Ba in and around RZ through highly precise Ba isotopic analyses. In particular, fissionogenic  $^{135}\text{Ba}$  and  $^{137}\text{Ba}$  are key isotopes in tracing the geochemical behavior of fissionogenic Cs. The timing of chemical fractionation between Ba and Cs, and the migration processes of Cs are discussed referring to the precise Ba isotopic data.

## **2. EXPERIMENTAL METHODS**

### **2.1. Samples**

Sixteen RZs have been found in the Oklo uranium deposit. Seven clay samples from the peripheral rocks of the Oklo RZ 16 and the Bangombé RZ, and six uraninite samples from the Oklo RZs 10 and 13 were used in this study. The samples were selected from RZs 10, 13 and 16, because it was expected that the samples would be less contaminated by non-fissionogenic elements on the basis of their little-weathered features (Gauthier-Lafaye et al., 1996; Hidaka and Holliger, 1998).

### 2.1.1. Clay

Clay samples were collected from the peripheral rocks of RZs. Three samples were taken from one of drill-cores PX8 which intersects RZ 16. The sub-number of the sample indicates the depth of the location in the drill-core. Figure 2(A) shows a stratigraphic section of the PX8 drill-core. The location of the RZ part in the PX8 drill-core corresponds to PX8-46 to 90. Samples PX8-03 and PX8-91 were adjacent to RZ16, and PX8-97 was 7 cm above the RZ. Three samples, D75-5, D75-10, and D75-23, were taken from clay parts adjacent to RZ 16. Figure 2(B) shows sampling locations in gallery D75 of RZ 16. BAX3.1190 was taken from a clay layer adjacent to the Bangombé RZ, as shown in Fig. 2(C). Previous studies revealed that secondarily formed minerals bearing fission products exist in the BAX3.1190 sample (Kikuchi et al., 2007).

### 2.1.2. RZ uraninite

Four samples, SF84.1469, 1480, 1485 and 1492, were taken from the SF84 borehole that intersects RZ 10. The whole rock analyses, including Ba isotopic measurements of SF84 samples, have been previously reported (Hidaka et al., 1993), and the data suggested that fissionogenic  $^{135}\text{Ba}$  and  $^{137}\text{Ba}$  isotopes behaved as Cs rather than Ba. It is known that the RZ part from the SF84 boring core is one of the least weathered sites in which fission products have been well preserved (Gauthier-Lafaye et al., 1996; Hidaka and Holliger, 1998). SD37-S2/CD (hereafter, SD37) was from the vicinity of RZ 16, and has the lowest  $^{235}\text{U}/^{238}\text{U}$  ratio (=0.004630) among the RZ samples (Hidaka and Holliger, 1998). D81N.26039 (hereafter, D81N) was taken from a terminal cross-cut in gallery D81N which intersects the lower part of RZ 10.

## 2.2. Chemical treatments

First, we attempted to find the Cs-enriched phase in thin-section samples from RZ uraninites and clays near RZs using an electron probe micro analyzer (EPMA), but were unsuccessful. Previous studies have show that Ba in the Oklo samples is, in most cases, highly diluted by large amounts of non-fissionogenic Ba possibly contaminated from outside of RZs (Brookins et al., 1975; Hidaka et al., 1992). Assuming that the fissionogenic Ba and contaminated non-fissionogenic Ba are at different sites in the crystalline structure of uraninite, they may be roughly separated by chemistry. In

addition, to obtain chemical information on Cs from Ba isotopic data, it is important to find the high-Cs/Ba phase in a sample. Therefore, in this study, sequential acid leaching treatment was carried out. The procedures were based on the method of Hidaka et al. (2001), which is useful for obtaining a high-Cs/Ba fraction from planetary materials. Fifty to a hundred mg of each powdered sample was leached using 10 mL of 0.1 M acetic acid-ammonium acetate, 0.1 M HCl, 2 M HCl and aqua regia, successively.

Each leachate was divided into two portions; one for thermal ionization mass spectrometry (TIMS) analysis to determine the isotopic composition of Ba, and another for inductively coupled plasma mass spectrometry (ICP-MS) analysis to determine the Cs and Ba elemental abundances.

For the TIMS analysis, barium was chemically separated using a conventional cation exchange method (Hidaka et al., 1993). Each leachate was dried once, and then dissolved in 2.5 mL of 2 M HCl. The sample solution was loaded onto a cation exchange packed column (Bio-rad AG50WX8, 200-400 mesh, H<sup>+</sup> form, 150 mm × φ4.0 mm). The column was washed with 5 mL of 2M HCl and 0.5 mL of 2M HNO<sub>3</sub>, successively, and then, the barium fraction was eluted with 3.0 mL of 2 M HNO<sub>3</sub>.

For the ICP-MS analysis, a portion of each leachate was evaporated to dryness once, and redissolved with 10 mL of 0.5 M HNO<sub>3</sub>. Then 0.05 g of 10 ppm-indium solution was added to the individual sample solutions as an internal standard element to optimize the analytical conditions for Cs and Ba measurements.

### 2.2.1. TIMS analysis

A VG54-30 thermal ionization mass spectrometer equipped with seven Faraday cups was used in this study. Data collection was performed with the static multimode. Seven Faraday cup collectors were configured to monitor <sup>134</sup>Ba, <sup>135</sup>Ba, <sup>136</sup>Ba, <sup>137</sup>Ba and <sup>138</sup>Ba, <sup>139</sup>La and <sup>140</sup>Ce. The monitoring of <sup>139</sup>La and <sup>140</sup>Ce during the Ba isotopic analyses is required to check the isobaric interferences of <sup>138</sup>La, <sup>136</sup>Ce and <sup>138</sup>Ce on <sup>136</sup>Ba and <sup>138</sup>Ba mass spectra. Two minor Ba isotopes, <sup>130</sup>Ba and <sup>132</sup>Ba, were not monitored in this study. Ba standard solution produced by SPEX Certi Prep. Inc., was used as a standard material in this study.

The Ba sample was loaded on a Re outer filament of a Re-triple filament

assembly. A  $^{138}\text{Ba}^+$  ion beam of  $(3.0\text{-}9.0)\times 10^{-11}$  A was obtained for more than 1 h from individual fractions.

$^{136}\text{Ba}$  is selected as a reference isotope for other Ba isotopes. In this study, we assumed that isotopic variation from the contribution of natural mass-dependent fractionation is much less than those from nuclear reactions, and all of the isotopic ratios are normalized to  $^{134}\text{Ba}/^{136}\text{Ba}$  for the correction of instrumental mass fractionation.  $^{134}\text{Ba}/^{136}\text{Ba}=0.307776$  has been often used as a normalization factor of Ba isotopic analyses (Hidaka et al., 2003). Although both  $^{134}\text{Ba}$  and  $^{136}\text{Ba}$  are non-fissiogenic isotopes, there is a possibility of significant isotopic variation of  $^{134}\text{Ba}/^{136}\text{Ba}$  isotopic ratio of the Oklo samples due to the contribution of neutron capture produced  $^{134}\text{Ba}$  by  $^{133}\text{Cs}(n,\gamma\beta^-)^{134}\text{Ba}$ . To determine the normalization factors of individual samples, total evaporation technique was adopted in this study. The data collection started from the intensity of  $^{138}\text{Ba}^+$  ion beam over  $1.0\times 10^{-11}$  A, and continued until the beam decayed to less than  $1.0\times 10^{-11}$  A. As the results, for the clay samples, all ratios except PX8-91#4 are normalized to  $^{134}\text{Ba}/^{136}\text{Ba}=0.307776$ . For the uraninite samples and PX8-91#4, as shown in Table 1, individual normalization factors were determined by the mean values of raw  $^{134}\text{Ba}/^{136}\text{Ba}$  isotopic data collected from individual total evaporation analyses.

### 2.2.2. ICP-MS analysis

A VG Plasma-Quad III was used in this study.  $^{133}\text{Cs}$ ,  $^{135}\text{Ba}$  and  $^{137}\text{Ba}$  were monitored in the analytical sequences. The detailed analytical procedures were based on the method of Shinotsuka et al. (1995). The difference in Ba isotopic abundances between standard materials and Oklo samples were corrected for the measurements of elemental abundances after the determination of isotopic abundances.

## 3. RESULTS AND DISCUSSION

Ba isotopic ratios of individual samples are shown in Table 1. Together with the isotopic ratios, the isotopic deviations relative to the standard values are also indicated in Table 1. The data are expressed in  $\epsilon$  unit as follows:

$$\epsilon_{i\text{Ba}} = \left\{ \frac{(^i\text{Ba}/^{136}\text{Ba})_{\text{sample}}}{(^i\text{Ba}/^{136}\text{Ba})_{\text{standard}}} - 1 \right\} \times 10^4$$

### 3.1. Fissiogenic and non-fissiogenic Ba

The elements of the Oklo samples consist of fissiogenic and non-fissiogenic origin. The retentivities of fissiogenic Ba components can be discussed on the basis of the variations of isotopic ratios. It is known that some kinds of clay minerals have specific abilities for the selective adsorption of alkaline and alkaline earth elements (Hidaka et al., 2007). Therefore, large deviations of  $^{135}\text{Ba}$ ,  $^{137}\text{Ba}$  and  $^{138}\text{Ba}$  in the clay samples near the RZs were expected as a result of the migration of fissiogenic Cs and Ba produced from RZs. However, as shown in Table 1(a), all of the leachate fractions, except PX8-9491#4, from the clay samples indicate no significantly large isotopic deviations ( $-1.5 < \epsilon < +1.8$ ). The data lead to the conclusion that fissiogenic Ba produced from RZs are not effectively adsorbed in clays. The only exceptional case showing significant isotopic deviations of Ba from clay was PX8-9491#4 as a leachate with aqua regia. Considering the enrichment of fissiogenic Ba from only the aqua regia leachate of PX8-9491, the fissiogenic Ba isotopes might have been incorporated into secondarily formed uranium minerals in the clay sample without large fractionation between Ba and U after the dissolution of RZ uraninite.

There is a possibility that fissiogenic  $^{135}\text{Ba}$ ,  $^{137}\text{Ba}$  and  $^{138}\text{Ba}$  (hereafter expressed as  $^{135}\text{Ba}_f$ ,  $^{137}\text{Ba}_f$  and  $^{138}\text{Ba}_f$ , respectively) behaved differently to each other, if significant chemical fractionation occurred between Cs and Ba. In order to estimate the degree of fractionation among the three fissiogenic Ba isotopes, all of the Ba isotopic data were treated by the following procedures.

(1) Assuming that  $^{134}\text{Ba}$  and  $^{136}\text{Ba}$  isotopes are only of non-fissiogenic origin, fissiogenic Ba components ( $\text{Ba}_f$ ) in individual samples can be calculated by subtracting the non-fissiogenic Ba component ( $\text{Ba}_n$ ) using the  $^{136}\text{Ba}$  isotopic abundance.

$${}^i\text{Ba}_{\text{sample}} = {}^i\text{Ba}_f + {}^i\text{Ba}_n \quad (i=135, 137, 138)$$

$${}^i\text{Ba}_{\text{sample}} = {}^i\text{Ba}_n \quad (i=134, 136)$$

(2) Calculated fissiogenic Ba is expressed as fissiogenic Ba isotopic ratios of relative  $^{137}\text{Ba}_f$  and  $^{138}\text{Ba}_f$  isotopic abundances normalized to  $^{135}\text{Ba}_f$ . The data set ( $^{137}\text{Ba}_f/^{135}\text{Ba}_f$  and  $^{138}\text{Ba}_f/^{135}\text{Ba}_f$ ) in each sample is used as fissiogenic Ba isotopic ratios.



$$\frac{{}^{137}\text{Ba}_f}{{}^{135}\text{Ba}_f} = \frac{\left(\frac{{}^{137}\text{Ba}}{{}^{136}\text{Ba}}\right)_{\text{sample}} - \left(\frac{{}^{137}\text{Ba}}{{}^{136}\text{Ba}}\right)_n}{\left(\frac{{}^{135}\text{Ba}}{{}^{136}\text{Ba}}\right)_{\text{sample}} - \left(\frac{{}^{135}\text{Ba}}{{}^{136}\text{Ba}}\right)_n} \quad \frac{{}^{138}\text{Ba}_f}{{}^{135}\text{Ba}_f} = \frac{\left(\frac{{}^{138}\text{Ba}}{{}^{136}\text{Ba}}\right)_{\text{sample}} - \left(\frac{{}^{138}\text{Ba}}{{}^{136}\text{Ba}}\right)_n}{\left(\frac{{}^{135}\text{Ba}}{{}^{136}\text{Ba}}\right)_{\text{sample}} - \left(\frac{{}^{135}\text{Ba}}{{}^{136}\text{Ba}}\right)_n}$$

Where,  $({}^{135}\text{Ba}/{}^{136}\text{Ba})_n$ ,  $({}^{137}\text{Ba}/{}^{136}\text{Ba})_n$  and  $({}^{138}\text{Ba}/{}^{136}\text{Ba})_n$  mean the non-fissiogenic values determined from the measurements of Ba standard material.

The calculated fissiogenic Ba isotopic ratios,  ${}^{137}\text{Ba}_f/{}^{135}\text{Ba}_f$  and  ${}^{138}\text{Ba}_f/{}^{135}\text{Ba}_f$ , of individual samples are listed in Table 2.

### 3.2. Correlation between ${}^{135}\text{Ba}$ excess and Cs/Ba elemental ratio

If  ${}^{135}\text{Cs}$  and  ${}^{137}\text{Cs}$  differentiated from Ba before the decay to  ${}^{135}\text{Ba}_f$  and  ${}^{137}\text{Ba}_f$ , respectively, the presently detected  ${}^{135}\text{Ba}_f$  and  ${}^{137}\text{Ba}_f$  may correlate with Cs rather than Ba. On the other hand, if there was no differentiation of Cs from Ba,  ${}^{135}\text{Ba}_f$  and  ${}^{137}\text{Ba}_f$  may correlate with Ba. Elemental abundances of Ba and Cs in individual leaching fractions measured by ICP-MS are listed in Table 3. Figure 3 shows a diagram between fissiogenic Ba ( ${}^{135}\text{Ba}_f$ ,  ${}^{137}\text{Ba}_f$  and  ${}^{138}\text{Ba}_f$ ) and elemental abundances of Ba or Cs in the acid leachates from the RZ samples (SF84-1469, -1480, -1485, -1492, D81N, and SD37).

Absolute amounts of  $\text{Ba}_f$  and  $\text{Ba}_n$  in each leachate of all samples can be determined from the isotopic ratios and elemental abundances of Ba. The results are listed in Table 4. In most cases, the leaching fractions from #1, #2 and #3 for the individual samples show very low contents of  $\text{Ba}_f$  (usually less than 1 ppm). Significant amounts of  $\text{Ba}_f$  were observed only in the aqua regia leachate #4 fractions of a series of SF84 (1.5 ppm to 44 ppm), which suggests that some  $\text{Ba}_f$  was originally incorporated into the uraninite crystalline structure. From the large deviation of data points in Fig. 3(A), the high concentration of Ba observed in D81N#2 (470 ppm), #3 (136 ppm), and SF84-1492#2 (160 ppm) were possibly from the contamination by non-fissiogenic component after reactor operation. In spite of the large Ba contents in these fractions, they contain very small amounts of  $\text{Ba}_f$ . Only the data points from fraction #4 show a better correlation between  $\text{Ba}_f$  and the Ba elemental abundances than other fractions. This suggests that the sequential acid treatment from #1 to #3 processes effectively removes the contamination of non-fissiogenic Ba component from the reactor uraninite.

On the other hand, as shown in Fig. 3(B),  $^{135}\text{Ba}_f$  and  $^{137}\text{Ba}_f$  show good correlations with the Cs contents rather than with those of Ba. In general, the Cs content in common crustal rocks are low. The content of Cs in the RZ uraninite shown as #4 leachates particularly from SF84 series is generally higher than those in other leachate fractions #1 to #3 (probably migrated out of the RZs as contamination) and in the peripheral rocks surrounding the RZs (Hidaka et al., 1993). Therefore, the RZ samples might have been negligibly contaminated by Cs from outside of the RZs.

It should be noted that the Cs concentrations in the leachates gradually increase with the progress of chemical processes. This suggests that Cs in leachates #3 and #4 might have been incorporated into the crystalline structure of clay minerals.

### 3.2.1. Chemical fractionation between Cs and Ba in RZs

It should be noted from Fig. 3(B) that absolute contents (ppm) of  $^{135}\text{Ba}_f$  (open circles) and  $^{137}\text{Ba}_f$  (open squares) are quantitatively equivalent to that of  $^{133}\text{Cs}$  in the #4 fractions from four SF84 samples. The fission product yield of  $^{133}\text{Cs}$  (6.70 % by  $^{235}\text{U}$  fission) is as high as those of  $^{135}\text{Ba}$  (6.54 %),  $^{137}\text{Ba}$  (6.32 %) and  $^{138}\text{Ba}$  (6.19%). Because Cs is a mono-isotopic element, its origin cannot be identified by isotopic study. However, considering the low background of original Cs contents in and around RZs, there is a high possibility that a large portion of Cs in the RZ uraninites is of fissiogenic origin. Assuming that the present Cs detected from the RZ uraninites (#4 fractions in individual samples) are fissiogenic, average values of  $^{135}\text{Ba}_f/\text{Cs}=1.1 \pm 0.1$  and  $^{137}\text{Ba}_f/\text{Cs}=1.3 \pm 0.1$  show a low degree of chemical fractionation (10 to 30 %) of  $^{135}\text{Ba}_f$  and  $^{137}\text{Ba}_f$  with  $^{133}\text{Cs}_f$ . The result indicate slight chemical fractionation between Cs and Ba after complete decays of  $^{135}\text{Cs}$  and  $^{137}\text{Cs}$  in RZ 10, considering that the retentivities of  $^{135}\text{Ba}_f/\text{Cs}$  and  $^{137}\text{Ba}_f/\text{Cs}$  are quite similar to fission yield ratios of  $^{135}\text{Ba}_f/^{133}\text{Cs}_f$  (0.98) and  $^{137}\text{Ba}_f/^{133}\text{Cs}_f$  (0.94). On the other hand, the average value of  $^{138}\text{Ba}_f/\text{Cs}=2.1 \pm 0.2$  reveals an enrichment of Ba in the fraction. These results suggest that slight chemical fractionation between Ba and Cs occurred when  $^{135}\text{Cs}$  and  $^{137}\text{Cs}$  were still alive, and a high degree of fractionation occurred after  $^{135}\text{Cs}$  and  $^{137}\text{Cs}$  completely decayed.

### 3.2.2. Chemical fractionation between Cs and Ba from outside of RZs

Ba isotopic variations in the clay samples from outside of RZs are not high enough to enable comparison with those in the RZ uraninites as shown in Table 1.

Because the isotopic abundance of  $^{138}\text{Ba}$  is originally high, it is difficult to quantitatively identify the migration of  $^{138}\text{Ba}_f$  from the isotopic data of most of the clay samples in this study. However, isotopic variations of  $^{135}\text{Ba}$  and  $^{137}\text{Ba}$  are sufficient to confirm the existence of  $^{135}\text{Ba}_f$  and  $^{137}\text{Ba}_f$ , although the isotopic excesses are  $\epsilon < +1.6$  in all of the samples except for PX8-9491#4.

Figures 4(A) and 4(B) are correlation diagrams of  $^{135}\text{Ba}_f$  and  $^{137}\text{Ba}_f$  with Ba and Cs contents, respectively, from leachates of clay samples from outside of RZs.  $^{135}\text{Ba}_f$  and  $^{137}\text{Ba}_f$  show a good correlation with the Ba contents rather than with those of Cs. The data for clays from outside of RZs indicate quite opposite result to those from RZ uraninites. Considering that both  $^{135}\text{Ba}_f$  and  $^{137}\text{Ba}_f$  in the clay have behaved as Ba, the  $^{135}\text{Ba}_f$  and  $^{137}\text{Ba}_f$  were primarily leaked out of RZs after complete decay of  $^{135}\text{Cs}$  and  $^{137}\text{Cs}$ . Although there is little correlation of  $^{135}\text{Ba}_f$  and  $^{137}\text{Ba}_f$  with Cs, the scattered data points shown in Fig. 4(B) are classified into two groups. ( $^{135}\text{Ba}_f + ^{137}\text{Ba}_f$ ) and Cs show a slight correlation in the lower Cs region (Cs < 1 ppm). On the other hand, little correlation is observed in the high Cs region (Cs > 1 ppm). A small portion of fissionogenic Cs might have moved out of the RZs, and been trapped in the clays.

An understanding of the Cs migration behavior on the basis of all data sources in this study is complicated, because there is little correlation between  $^{135}\text{Ba}_f + ^{137}\text{Ba}_f$  and Cs. However, the data from individual drill core samples may provide a hint for understanding the Cs behavior. The data from three kinds of drill-core samples are individually shown in Fig. 5. In the case of BAX1190 from the BAX03 drill core, the isotopic excesses of  $^{135}\text{Ba}$  and  $^{137}\text{Ba}$  are very small ( $\epsilon_{^{135}\text{Ba}} < +0.82$ ,  $\epsilon_{^{137}\text{Ba}} < +0.97$ ) and the data are from only one sample. However, the data show a slight correlation between  $^{135}\text{Ba}_f + ^{137}\text{Ba}_f$  and Cs (Fig. 5(A)). Because the Bangombé RZ has been overlain by the clay layer, some of the fissionogenic Cs leached out of the RZ might have been selectively adsorbed on the clay.

As shown in Figs. 5(B) and 5(C), the data of a series of samples from D75 at RZ 13 and PX8 RZ 16 show a similar trend. Better correlation between  $^{135}\text{Ba}_f + ^{137}\text{Ba}_f$  and Cs is observed in the low Cs region (Cs < 1) rather than the high Cs region (Cs > 1). The data of the low Cs regions mainly consist of those of #1 and #2 leachates, while those of the high Cs regions are from #3 and #4 leachates. The data suggest a difference in the adsorption sites of Cs on the clay minerals. Ba and Cs in leaching fractions #1 and #2, having better correlation, were easily dissolved by weak acid

reagents, while those in #3 and #4 were leached out by strong acids.

### 3.3. Fissiogenic Ba isotopic patterns

Fissiogenic Ba isotopic patterns can be used to elucidate the chemical fractionation between Ba and Cs and the timing of its occurrence (Hidaka et al., 1993). Considering the fission product yields of  $^{135}\text{Ba}$ ,  $^{137}\text{Ba}$  and  $^{138}\text{Ba}$ , their isotopic abundances are almost equivalent if their fission products have well retained without fractionation. Isotopic abundances of  $^{135}\text{Ba}_f$ ,  $^{137}\text{Ba}_f$  and  $^{138}\text{Ba}_f$  in the samples vary with the timing and degree of chemical fractionation between Cs and Ba because of a large difference in the half-lives of  $^{135}\text{Cs}$  and  $^{137}\text{Cs}$  as precursors of  $^{135}\text{Ba}_f$  and  $^{137}\text{Ba}_f$ , respectively.

Considering the chemical fractionation between Cs and Ba by single stage at  $t=T$ , fissiogenic Cs ( $\text{Cs}_f$ ) and Ba ( $\text{Ba}_f$ ) can be defined as a function of time.

When  $0 < t < T$ ,

$${}^i\text{Cs}_f(t) = {}^i\text{Cs}_{f0} \cdot e^{-\lambda_i t}$$

$${}^i\text{Ba}_f(t) = {}^i\text{Cs}_{f0} \cdot (1 - e^{-\lambda_i t})$$

where  $i=135$  and  $137$ ,  ${}^i\text{Cs}_{f0}$  is the initial abundance of fissiogenic  ${}^i\text{Cs}_f$ , and  $\lambda_i$  is the decay constant of  ${}^i\text{Cs}$ .

When  $t > T$ ,

$${}^i\text{Cs}_f(t) = f \cdot {}^i\text{Cs}_{f0} \cdot e^{-\lambda_i t}$$

$${}^i\text{Ba}_f(t) = {}^i\text{Cs}_{f0} \cdot \left\{ 1 - (1-f)e^{-\lambda_i T} - fe^{-\lambda_i t} \right\}$$

where,  $f$  is the fractionation factor of Cs relative to Ba ( $f < 1$  for Cs lost, and  $f > 1$  for Cs gain).

Therefore, two isotopic ratios,  $^{137}\text{Ba}_f/^{135}\text{Ba}_f$  and  $^{138}\text{Ba}_f/^{135}\text{Ba}_f$ , obtained by subtracting the non-fissiogenic Ba isotopic component, are shown as

$$\frac{{}^{137}\text{Ba}_f}{{}^{135}\text{Ba}_f} = \frac{{}^{137}\text{Cs}_{f0}}{{}^{135}\text{Cs}_{f0}} \cdot \frac{\left\{ 1 - (1-f)e^{-\lambda_{137}T} - fe^{-\lambda_{137}t} \right\}}{\left\{ 1 - (1-f)e^{-\lambda_{135}T} - fe^{-\lambda_{135}t} \right\}} \quad \text{Eq.(1)}$$

$$\frac{{}^{138}\text{Ba}_f}{{}^{135}\text{Ba}_f} = \frac{{}^{138}\text{Ba}_{f0}}{{}^{135}\text{Cs}_{f0}} \cdot \frac{1}{\left\{ 1 - (1-f)e^{-\lambda_{135}T} - fe^{-\lambda_{135}t} \right\}} \quad \text{Eq.(2)}$$

where  ${}^{137}\text{Cs}_{f0}/{}^{135}\text{Cs}_{f0}=6.19/6.54$  and  ${}^{138}\text{Ba}_{f0}/{}^{135}\text{Cs}_{f0}=6.77/6.54$  are used for the fission product yield data from  $^{235}\text{U}$  fission (England and Rider, 1994).  $t=0$  is the time at the

end of reactor operation, and  $t=2 \times 10^9$  yrs corresponds to the present time.

### 3.3.1. RZ uraninites

As shown in Table 2, fissionogenic Ba patterns of the Oklo RZ samples are classified into three types.

(1) Type 1 ( $^{137}\text{Ba}_f/^{135}\text{Ba}_f=1.0-1.2$ ,  $^{138}\text{Ba}_f/^{135}\text{Ba}_f=1.4-2.0$ )

Similar abundances between  $^{135}\text{Ba}_f$  and  $^{137}\text{Ba}_f$ , and slight excess of  $^{138}\text{Ba}_f$  are observed in almost all of the leachates (SF84.1469#1~4, SF84.1480#1~4, SF84.1485#1~3, SF84.1492#1~3, SD37#2~4, D81N#4). The pattern suggests early fractionation between Cs and Ba, at least when both radioactive  $^{135}\text{Cs}$  and  $^{137}\text{Cs}$  were still alive, because  $^{135}\text{Ba}_f$  and  $^{137}\text{Ba}_f$  isotopic abundances were not fractionated in spite of the large differences in the half-lives of  $^{135}\text{Cs}$  and  $^{137}\text{Cs}$ . In addition, the fractionation degree of Ba relative to Cs in the fractions was at most 2.0 times.

(2) Type 2 ( $^{137}\text{Ba}_f/^{135}\text{Ba}_f=1.6$ ,  $^{138}\text{Ba}_f/^{135}\text{Ba}_f=8.9$ )

Large excess of  $^{138}\text{Ba}_f$  relative to  $^{135}\text{Ba}_f$  and  $^{137}\text{Ba}_f$  and slight differentiation between  $^{135}\text{Ba}_f$  and  $^{137}\text{Ba}_f$  were observed only in D81N#2. This is a case of large degree of differentiation between Cs and Ba ( $f>1$ ). In this fraction, the difference in isotopic abundances between  $^{135}\text{Ba}_f$  and  $^{137}\text{Ba}_f$  is evidence of chemical fractionation between  $^{135}\text{Cs}$  and Ba after the decay of  $^{137}\text{Cs}$ . However, contribution of fissionogenic Ba component in D81N#2 is very low because of the existence of large amount of non-fissionogenic Ba component (470 ppm shown in Table 3). Therefore, the estimated fissionogenic Ba isotopic ratios,  $^{137}\text{Ba}_f/^{135}\text{Ba}_f$  and  $^{138}\text{Ba}_f/^{135}\text{Ba}_f$ , of this sample include larger analytical uncertainties than the other data.

(3) Type 3 ( $^{137}\text{Ba}_f/^{135}\text{Ba}_f=0.8-0.95$ ,  $^{138}\text{Ba}_f/^{135}\text{Ba}_f=0$ )

A slightly low excess of  $^{137}\text{Ba}_f$  relative to  $^{135}\text{Ba}_f$  and no  $^{138}\text{Ba}_f$  were observed in both D81N#1 and D81N#3, suggesting differentiation from each other. This is another case of a large degree of differentiation between Cs and Ba. In the type 2 fraction, enrichment of the Ba fraction as a result of chemical fractionation between Cs and Ba is observed. However, as an opposite effect resulting from the Cs-Ba chemical fractionation, the enrichment of Cs is observed.

Major phases in the RZ uraninites show fissionogenic Ba isotopic patterns of type 1. Isotopic patterns of types 2 and 3 are observed only in soluble phases (#1~3) in the D81N sample. The study of fission product distributions in spent fuel reveals that

fissionogenic Cs migrates to grain boundaries, fractures and the gap between the fuel pellets and the surrounding cladding (Shoosmith, 2000; Buck et al., 2004). Therefore, the existence of fissionogenic Cs from the D81N sample is reasonable, considering that sample D81N is from the boundary between RZ and wall rock.

The Ba fissionogenic patterns ( $^{137}\text{Ba}_f/^{135}\text{Ba}_f$  and  $^{138}\text{Ba}_f/^{135}\text{Ba}_f$  ratios) can provide temporal and chemical constraints for the differentiation between Cs and Ba. Figure 6 shows the time dependences of  $^{137}\text{Ba}_f/^{135}\text{Ba}_f$  and  $^{138}\text{Ba}_f/^{135}\text{Ba}_f$  ratios with different value of the fractionation factor  $f$ . The variation curves of  $^{137}\text{Ba}_f/^{135}\text{Ba}_f$  with different  $f$  shown in Fig. 6(A) have two focal points around  $T < 1$  and  $T > 10^7$  with somewhat flat regions between two focal points. Therefore, even if differentiation factor  $f$  is determined, there are apparently two solutions for  $T$ . On the other hand,  $^{138}\text{Ba}_f/^{135}\text{Ba}_f$  data shown in Fig. 6(B) always provide upper or lower limitation for  $f$  and  $T$ .  $f < 0.739$  and  $T < 4 \times 10^6$  for type 1,  $f < 0.116$  and  $T < 4 \times 10^5$  for type 2,  $f > 10.3$  and  $T < 4 \times 10^6$  for type 3 were estimated only from the  $^{138}\text{Ba}_f/^{135}\text{Ba}_f$  data in Fig. 6(B). More critical constraints can put on  $f$  and  $T$  from the combination with  $^{137}\text{Ba}_f/^{135}\text{Ba}_f$  and  $^{138}\text{Ba}_f/^{135}\text{Ba}_f$ . It should be noted that that for the range of the differentiation time  $T$  there are two separated regions for given data  $f$  from the  $^{138}\text{Ba}_f/^{135}\text{Ba}_f$  data. The  $^{137}\text{Ba}_f/^{135}\text{Ba}_f$  data of type 2 provide  $T < 5$  and  $2 \times 10^6 < T < 3 \times 10^6$  for  $f < 0.116$  given by the  $^{138}\text{Ba}_f/^{135}\text{Ba}_f$  data. Since  $T < 4 \times 10^5$  is given by the  $^{138}\text{Ba}_f/^{135}\text{Ba}_f$  data of type 2,  $T < 5$  is reasonable to satisfy both of the two isotopic ratios. Similar results can be obtained for types 1 and 3. The  $^{137}\text{Ba}_f/^{135}\text{Ba}_f$  data of type 3 give  $T < 8$  and  $T > 1 \times 10^7$  by  $f > 10.3$ , while the  $^{138}\text{Ba}_f/^{135}\text{Ba}_f$  data give  $T < T < 3 \times 10^5$ . Therefore we can adopt  $T < 8$  for type 3. In the case of type 1, using  $f < 0.739$  and  $T < 4 \times 10^6$  from the  $^{138}\text{Ba}_f/^{135}\text{Ba}_f$  data,  $T < 20$  were calculated from individual  $^{137}\text{Ba}_f/^{135}\text{Ba}_f$  data.

Our calculation shown in Fig. 6 is simply based on the single stage by short pulse fractionation. Considering the heterogeneity of Cs and Ba elemental abundances in the samples used in this study (Table 3), the fractionation event should be more complicated and occurred by several stages during and after reactor cycling. However, it is meaningful to find fractionation processes to produce variable  $^{137}\text{Ba}_f/^{135}\text{Ba}_f$  and  $^{138}\text{Ba}_f/^{135}\text{Ba}_f$  ratios by our simple simulation.

Considering the duration of the RZ operation, which is estimated as  $10^5$  to  $10^6$  yrs (e.g., Gauthier-Lafaye et al., 1996; Hidaka and Holliger 1998), the pulse used for the fractionation modeling in this study seems too short to determine the fractionation

conditions. Recent Xe and Kr isotopic study using selective laser extraction technique also provides evidence of the early differentiation of fissionogenic Te and I from  $\text{UO}_2$  and the subsequent selective adsorption onto aluminous hydroxyl phosphate (Meshik et al., 2004). Interestingly, the Xe isotopic study defines a cycling operation for the RZ with 30 min active pulses separated by 2.5 h periods. Therefore, our simple calculation also shows a good approximation for tracing the behavior of fissionogenic Cs isotopes with different half-lives, although multiple-stage and/or continuous fractionation should be considered for practical usage.

### 3.3.2. Clays

Besides the leachates from the RZ uraninites, some leachates (PX8.03#1-4, PX8.9491#1 and #4) from the clay samples also show small but significant isotopic excesses. The fission patterns of the clay sample shown in Table 2(a) are, in most cases, different from the fission patterns (types 1 to 3) typically observed for RZ uraninites. Although isotopic excesses of  $^{135}\text{Ba}_f$  and  $^{137}\text{Ba}_f$  are observed, those of  $^{137}\text{Ba}_f$  are not clearly detected from most of the clay samples (PX8.03#1-4 and PX8.9491#1). This result suggests that fissionogenic Cs ( $^{135}\text{Cs}$  and  $^{137}\text{Cs}$ ) was trapped in the clay after chemical differentiation between Cs and Ba. Subsequently, fissionogenic  $^{135}\text{Cs}$  and  $^{137}\text{Cs}$  decayed and were detected as isotopic excesses for  $^{135}\text{Ba}_f$  and  $^{137}\text{Ba}_f$ , respectively. However, only the fission pattern of PX8.9491#4 resembles those of RZ sample shown as type 1. Considering that PX8.9491 faced the boundary of RZ 16, a small amount of RZ uraninite might have dissolved with little chemical fractionation, and then re-crystallized in sample PX8.9491. Therefore, the  $\text{Ba}_f$ -enriched fraction was found in the leachate of aqua regia that effectively dissolves uraninite, and its fission pattern resembles those of RZ.

## 4. CONCLUSIONS

Fissionogenic Ba isotopic compositions of the RZ samples can put temporal constraints for chemical fractionation between Cs and Ba in the RZs. RZ uraninites show significant isotopic deviations of  $^{135}\text{Ba}$ ,  $^{137}\text{Ba}$  and  $^{138}\text{Ba}$  derived from fission. In particular, large amounts of fissionogenic Ba were found in aqua regia fractions (#4) of SF84 samples, suggesting that 10-20 % of fissionogenic Ba is retained in the little weathered uraninite. On the other hand, the samples from D81N and SD37 show

much lower retentivities of Ba than those from SF84. Considering the degree of deviation of Ba isotopes and the elemental concentrations of Ba in individual leachates, Ba contaminant of non-fissiogenic origin was sufficiently removed in the first to third stages of sequential acid leaching processes.

The fissiogenic Ba isotopic patterns of the RZ uraninites are classified into three types showing different timings and magnifications of differentiation. The isotopic signatures suggest early differentiation of Cs and Ba less than 20 years after the production of fissiogenic Cs and Ba. We expected significant isotopic excesses of  $^{135}\text{Ba}$  and  $^{137}\text{Ba}$  in the clay samples from peripheral rocks of the RZs, on the basis of the selective adsorption of Cs on clay minerals after the migration of Cs out of the RZs. However, only small excesses of  $^{135}\text{Ba}$  ( $\epsilon < +1.8$ ) and/or  $^{137}\text{Ba}$  ( $\epsilon < +1.3$ ) were identified in some of the clay samples, which might have been a result of the selective adsorption of  $^{135}\text{Cs}$  and  $^{137}\text{Cs}$  migrating from the reactors by differentiation.

Although we paid attention to the Cs-Ba system to characterize the geochemical behavior of fissiogenic Ba in this study, influence of the radioactive precursors of fissiogenic Ba other than Cs is also important for the retentivity of fissiogenic Ba. The chemical properties of I and Xe as the radioactive precursors are quite different from Cs and Ba, even if their half-lives in the fission chains are shorter than several hours. More systematic isotopic studies including I and Xe are needed to elucidate the detailed migration process of fissiogenic Ba.

### **Acknowledgements**

We are grateful to Drs. S. Yoneda (National Museum of Nature and Science, Tokyo) and Y. Takahashi (Hiroshima Univ.) for their technical supports with TIMS and ICP-MS analyses. Helpful comments and constructive reviews by J.R. DeLaeter (Curtin Univ. of Tech., Perth) and two anonymous journal reviewers were useful to improve the first draft of this paper. This study was financially supported by a Grant-in-Aid for Scientific Research of Japan Society for the Promotion of Science (to H.H., No. 17204051).



## REFERENCES

- Brookins D.G., Lee M.J., Mukhopadhyay B., Bolivar S.L. (1975) Search for fission-produced Rb, Sr, Cs and Ba at Oklo. Int. Symp. of the Oklo Phenomenon. IAEA, SM-204/3.
- Buck E.C., Hanson B.D., McNamara B.K. (2004) The geochemical behavior of Tc, Np and Pu in spent nuclear fuel in an oxidizing environment. In: Gieré R., Stille P. (eds.) Energy, Waste, and the Environment: a Geochemical Perspective. The Geological Society of London Special Publication 236: pp65-88.
- Commans, R.N.J., Hockley, D.E. (1992) Kinetics of cesium sorption on illite. *Geochim. Cosmochim. Acta* **56**, 1157-1164.
- DeLaeter, J.R., Hidaka, H. (2007) The role of mass spectrometry to study the Oklo-Bangombé natural reactors. *Mass Spectrometry Reviews* **26**, 683-712.
- England, T.R., Rider, B.F. (1994) LA-UR-94-3106, ENDF-349.
- Gauthier-Lafaye, F., Holliger, P., Blanc, P.-L. (1996) Natural fission reactors in the Franceville basin, Gabon: A review of the conditions and results of a “critical event” in a geologic system. *Geochim. Cosmochim. Acta* **60**, 4831-4852.
- Hidaka, H., Holliger, P. (1998) Geochemical and neutronic characteristics of the natural fossil fission reactors at Oklo and Bangombé, Gabon. *Geochim. Cosmochim. Acta* **62**, 89-108.
- Hidaka H., Konishi T., Masuda A. (1992) Reconstruction of cumulative fission yield curve and geochemical behaviors of fissiogenic nuclides in the Oklo natural reactors. *Geochem. J.*, **26**, 227-239.
- Hidaka H., Holliger P., Masuda A. (1993) Evidence of fissiogenic Cs estimated from Ba isotopic deviations in an Oklo natural reactor zone. *Earth Planet. Sci. Lett.*, **114**, 391-396.
- Hidaka H., Ohta Y., Yoneda S., DeLaeter J.R. (2001) Isotopic search for live  $^{135}\text{Cs}$  in the early solar system and possibility of  $^{135}\text{Cs}$ - $^{135}\text{Ba}$  chronometer. *Earth Planet. Sci. Lett.* **193**, 459-466.
- Hidaka H., Ohta Y., Yoneda S. (2003) Nucleosynthetic components of the early solar system inferred from Ba isotopic compositions in carbonaceous chondrites. *Earth Planet. Sci. Lett.* **214**, 455-466.
- Hidaka, H., Janeczek, J., Skomurski, F.N., Ewing, R., Gauthier-Lafaye, F. (2005)

- Geochemical fixation of rare earth elements into secondary minerals in sandstones beneath a natural fission reactor at Bangombé, Gabon. *Geochim. Cosmochim. Acta* **69**, 685-694.
- Hidaka H., Horie K., Gauthier-Lafaye F. (2007) Transport and selective uptake of radium into natural clay minerals. *Earth Planet. Sci. Lett.* **264**, 167-176.
- Horie, K., Hidaka, H., Gauthier-Lafaye, F. (2004) Isotopic evidence for trapped fissionogenic REE and nucleogenic Pu in apatite and Pb evolution at the Oklo natural reactor. *Geochim. Cosmochim. Acta* **68**, 115-125.
- Kikuchi, M., Hidaka, H., Horie, K., Gauthier-Lafaye, F. (2007) Redistribution of REE, Pb and U by supergene weathering studied from in-situ isotopic analyses of the Bangombé natural reactor, Gabon. *Geochim. Cosmochim. Acta* **71**, 4716-4726.
- Kleykamp K. (1985) The chemical state of fission products in oxide fuels. *J. Nucl. Mat.*, **131**, 221-246.
- Meshik, A.P., Hohenberg, C.M., Pravdivtseca, O.V. (2004) Record of cycling operation of the natural nuclear reactor in the Oklo/Okelobondo area in Gabon. *Phys. Rev. Lett.* **93**, 182302-1-4.
- Poinssot, C., Baeyens, B., Bradbury, M.H. (1999) Experimental and modeling studies of Cs sorption on illite. *Geochim. Cosmochim. Acta* **63**, 3217-3227.
- Sawhney, B.L. (1970) Potassium and cesium ion selectivity in relation to clay mineral structure. *Clays Clay Mineral.* **18**, 47-52.
- Shinotsuka K., Hidaka H., Ebihara M. (1995) Detailed abundances of rare earth elements, thorium and uranium in chondritic meteorites: An ICP-MS study. *Meteoritics* **30**, 694-699.
- Shoesmith, D.W. (2000) Fuel corrosion processes under waste disposal conditions. *J. Nucl. Mat.* **282**, 1-31.
- Vejsada, J., Hradil, D., Randa, Z., Jelinek, E., Stulik, K. (2005) Adsorption of cesium on Czech smectite-rich clays – A comparative study. *Appl. Clay Sci.* **30**, 53-66.

## Figure captions

Fig. 1. A part of the nuclear chart between iodine (Z=53) and barium (Z=56). Only stable isotopes and long-lived isotopes with half lives > 10 years are shown in the figure. The arrows in the figure indicate the paths of  $\beta^-$  decays.

Fig. 2. (a) The location of RZs at the Oklo uranium deposit. (b) Stratigraphic log of the PX8 drill-core at RZ16. (c) Cross section of gallery SD37 at RZ 13 and the location of the samples D75-10 and D75-23. (d) Stratigraphic log of the drill-core BAX3 at the Bangombe RZ.

Fig. 3. Correlation diagrams of (A) fissiogenic Ba ( $^{135}\text{Ba}_f$ ,  $^{137}\text{Ba}_f$  and  $^{138}\text{Ba}_f$ ) vs. Ba content (ppm), and (B) fissiogenic Ba vs. Cs content (ppm) in chemical leachates from RZ uraninites. Absolute amounts of  $^{135}\text{Ba}_f$ ,  $^{137}\text{Ba}_f$  and  $^{138}\text{Ba}_f$  are calculated by subtraction of non-fissiogenic Ba components (see text).

Fig. 4. Correlation diagrams of (A) fissiogenic Ba ( $^{135}\text{Ba}_f$  and  $^{137}\text{Ba}_f$ ) vs. Ba content (ppm), and (B) fissiogenic Ba vs. Cs content (ppm) in chemical leachates from clay samples. Absolute amounts of  $^{135}\text{Ba}_f$  and  $^{137}\text{Ba}_f$  are calculated by subtraction of non-fissiogenic Ba components (see text).

Fig. 5. Correlation diagrams of fissiogenic Ba ( $^{135}\text{Ba}_f$  and  $^{137}\text{Ba}_f$ ) vs. Cs content (ppm) in individual sampling sites: (A) BAX3 at Bangombé, (B) D75 at RZ 13, and (C) PX8 at RZ 16.

Fig. 6. Time-dependences of fissiogenic Ba ratios ( $^{137}\text{Ba}_f/^{135}\text{Ba}_f$  and  $^{138}\text{Ba}_f/^{135}\text{Ba}_f$ ) with different fractionation factor ( $f=0.1, 0.2, 0.5, 1, 2, 10, 100$ ). Shaded zones in the figures indicate the values of types 1,2, and 3. Calculations are based on the equations (1) and (2) in the text.

Table 1. Ba isotopic deviations of (a) clay, and (b) uraninite samples in and around the Oklo and Bangombé RZs.

(a) Clay

sample	$^{135}\text{Ba}/^{136}\text{Ba}$	$^{137}\text{Ba}/^{136}\text{Ba}$	$^{138}\text{Ba}/^{136}\text{Ba}$	$\epsilon_{135\text{Ba}}$	$\epsilon_{137\text{Ba}}$	$\epsilon_{138\text{Ba}}$
<b>BAX1190</b>						
#1	0.839378 (14)	1.428827 (31)	9.12714 (28)	+0.82 ± 0.21	-0.08 ± 0.26	-1.46 ± 0.36
#2	0.839354 (10)	1.428838 (19)	9.12812 (20)	+0.54 ± 0.17	-0.01 ± 0.20	-0.39 ± 0.29
#3	0.839367 (8)	1.428792 (20)	9.12769 (19)	+0.69 ± 0.15	-0.33 ± 0.20	-0.86 ± 0.28
#4	0.839307 (11)	1.428977 (23)	9.12893 (22)	-0.02 ± 0.18	+0.97 ± 0.22	+0.50 ± 0.31
<b>D75-5</b>						
#1	0.839414(7)	1.428899(15)	9.12815(16)	+1.25 ± 0.15	+0.42 ± 0.18	-0.01 ± 0.25
#2	0.839409(7)	1.428809(12)	9.12817(12)	+1.19 ± 0.14	-0.21 ± 0.17	-0.34 ± 0.23
#3	0.839412(7)	1.428937(14)	9.12875(13)	+1.22 ± 0.15	+0.69 ± 0.17	+0.30 ± 0.24
#4	0.839448(10)	1.428917(25)	9.12780(23)	+1.66 ± 0.17	+0.55 ± 0.23	-0.74 ± 0.31
<b>D75-10</b>						
#1	0.839417 (8)	1.428934 (18)	9.12836 (16)	+1.29 ± 0.16	+0.66 ± 0.19	-0.13 ± 0.26
#2	0.839412 (7)	1.428895 (12)	9.12857 (13)	+1.23 ± 0.15	+0.39 ± 0.17	+0.11 ± 0.24
#3	0.839447 (8)	1.428834 (16)	9.12784 (13)	+1.64 ± 0.16	-0.03 ± 0.18	-0.69 ± 0.24
#4	0.839435 (4)	1.428802 (9)	9.12824 (9)	+1.50 ± 0.14	-0.26 ± 0.16	-0.26 ± 0.21
<b>D75-23</b>						
#1	0.839434 (9)	1.428877 (15)	9.12785 (13)	+1.49 ± 0.16	+0.27 ± 0.18	-0.68 ± 0.24
#2	0.839423 (14)	1.428851 (14)	9.12828 (13)	+1.36 ± 0.21	+0.08 ± 0.17	-0.21 ± 0.24
#3	0.839415 (6)	1.428821 (13)	9.12853 (11)	+1.26 ± 0.15	-0.13 ± 0.17	+0.06 ± 0.23
#4	0.839462 (8)	1.429011 (18)	9.12874 (18)	+1.82 ± 0.16	+1.20 ± 0.19	+0.29 ± 0.28
<b>PX8-03</b>						
#1	0.839432 (9)	1.428899 (20)	9.12823 (17)	+1.22 ± 0.17	+0.76 ± 0.20	-0.16 ± 0.27
#2	0.839413 (7)	1.428899 (16)	9.12859 (15)	+0.99 ± 0.15	+0.75 ± 0.18	+0.23 ± 0.25
#3	0.839409 (10)	1.428932 (21)	9.12821 (19)	+0.94 ± 0.17	+0.99 ± 0.21	-0.19 ± 0.28
#4	0.839428 (10)	1.428976 (16)	9.12878 (14)	+1.17 ± 0.17	+1.29 ± 0.18	+0.44 ± 0.24
<b>PX8-9491</b>						
#1	0.839459 (6)	1.428921 (11)	9.12865 (9)	+1.54 ± 0.14	+0.91 ± 0.16	+0.30 ± 0.21
#2	0.839412 (6)	1.428830 (16)	9.12782 (15)	+0.98 ± 0.14	+0.27 ± 0.18	-0.62 ± 0.25
#3	0.839423 (5)	1.428853 (13)	9.12822 (10)	+1.24 ± 0.13	+0.08 ± 0.17	-0.12 ± 0.16
#4	0.847117 (7)	1.436749 (13)	9.13890 (10)	+92.78 ± 0.16	+55.35 ± 0.18	+11.58 ± 0.27
<b>PX8-9794</b>						
#1	0.839420 (7)	1.428894 (16)	9.12801 (14)	+1.07 ± 0.16	+0.37 ± 0.19	-0.35 ± 0.29
#2	0.839427 (10)	1.428848 (21)	9.12730 (22)	+1.16 ± 0.18	+0.05 ± 0.21	-1.13 ± 0.35
#3	0.839373 (12)	1.428997 (19)	9.12865 (19)	+0.51 ± 0.20	+1.09 ± 0.20	+0.34 ± 0.33
#4	0.839354 (13)	1.429003 (33)	9.12835 (33)	+0.29 ± 0.21	+1.13 ± 0.28	+0.02 ± 0.44

All ratios except PX8-9491#4 are normalized to  $^{134}\text{Ba}/^{136}\text{Ba}=0.307776$ .

The data of PX8-9491#4 are normalized to  $^{134}\text{Ba}/^{136}\text{Ba}=0.308855$ .

The numbers in parentheses are analytical errors ( $2\sigma$  of the means) of the last digits indicated.

## (b) uraninite

sample	$^{134}\text{Ba}/^{136}\text{Ba}$	$^{135}\text{Ba}/^{136}\text{Ba}$	$^{137}\text{Ba}/^{136}\text{Ba}$	$^{138}\text{Ba}/^{136}\text{Ba}$	$\epsilon_{^{135}\text{Ba}}$	$\epsilon_{^{137}\text{Ba}}$	$\epsilon_{^{138}\text{Ba}}$
SF84-1469							
#1	0.308776	0.845686 (28)	1.435312 (54)	9.13820 (57)	+76.14 ± 0.35	+45.42 ± 0.40	+10.32 ± 0.67
#2	0.308790	0.845475 (11)	1.435079 (22)	9.13727 (20)	+73.63 ± 0.18	+43.79 ± 0.20	+9.30 ± 0.32
#3	0.308809	0.845108 (16)	1.434793 (30)	9.13703 (29)	+69.01 ± 0.24	+42.08 ± 0.26	+10.19 ± 0.42
#4	0.315960	1.229429 (18)	1.839880 (28)	9.76243 (25)	+4647 ± 0.27	+2877 ± 0.26	+694 ± 0.35
SF84-1480							
#1	0.308858	0.847028 (14)	1.436865 (30)	9.14133 (30)	+92.13 ± 0.21	+56.29 ± 0.25	+13.75 ± 0.40
#2	0.309199	0.884190 (8)	1.475894 (16)	9.20304 (16)	+534.4 ± 0.16	+329.3 ± 0.18	+81.67 ± 0.27
#3	0.320624	1.355140 (41)	1.989358 (41)	10.05812 (27)	+6146 ± 0.53	+3923 ± 0.36	+1019 ± 0.41
#4	0.320527	1.306373 (20)	1.935983 (44)	9.97714 (31)	+5564 ± 0.3	+3549 ± 0.3	+929.7 ± 0.4
SF84-1485							
#1	0.308246	0.858641 (4)	1.448587 (11)	9.15957 (10)	+230.5 ± 0.13	+138.3 ± 0.15	+33.73 ± 0.25
#2	0.309360	0.870728 (6)	1.461034 (10)	9.17799 (8)	+374.3 ± 0.16	+225.7 ± 0.18	+55.07 ± 0.28
#3	0.310913	0.940737 (8)	1.534296 (19)	9.29583 (19)	+1208 ± 0.17	+738.0 ± 0.19	+183.3 ± 0.29
#4	0.354573	2.846094 (27)	3.797718 (56)	12.98104 (34)	+23909 ± 0.5	+16579 ± 0.5	+4220 ± 0.5
SF84-1492							
#1	0.309074	0.891656 (16)	1.482818 (31)	9.21075 (28)	+623.9 ± 0.2	+377.9 ± 0.2	+89.80 ± 0.38
#2	0.308786	0.875963 (12)	1.466498 (24)	9.18334 (23)	+436.6 ± 0.2	+264.0 ± 0.2	+60.92 ± 0.37
#3	0.309101	0.867592 (9)	1.457881 (24)	9.17245 (20)	+336.6 ± 0.2	+203.2 ± 0.2	+48.17 ± 0.30
#4	0.357952	3.221712 (34)	4.246379 (43)	13.56868 (26)	+28384 ± 0.6	+19719 ± 0.5	+4864 ± 0.41
D81N260392							
#1	0.307776	0.839559 (20)	1.429073 (44)	9.12808 (46)	+3.15 ± 0.27	+1.76 ± 0.34	-0.76 ± 0.56
#2	0.307776	0.839439 (11)	1.428981 (20)	9.12883 (21)	+1.47 ± 0.19	+1.40 ± 0.21	+1.21 ± 0.35
#3	0.307776	0.839489 (8)	1.42897 (15)	9.12844 (14)	+1.82 ± 0.15	+0.85 ± 0.17	-0.05 ± 0.25
#4	0.308574	0.842754 (7)	1.432582 (18)	9.13395 (17)	+40.78 ± 0.09	+26.74 ± 0.16	+6.25 ± 0.23
SD37S2/CD							
#1	0.307776	0.839330 (11)	1.428791 (21)	9.12838 (22)	+0.41 ± 0.18	-0.22 ± 0.20	-0.43 ± 0.33
#2	0.307776	0.841258 (9)	1.430862 (16)	9.13172 (15)	+23.14 ± 0.17	+14.56 ± 0.19	+4.37 ± 0.31
#3	0.307776	0.841071 (5)	1.430684 (14)	9.13129 (13)	+20.67 ± 0.14	+12.85 ± 0.16	+3.08 ± 0.25
#4	0.308510	0.844681 (19)	1.434363 (24)	9.13647 (19)	+63.74 ± 0.23	+39.20 ± 0.19	+9.01 ± 0.25

The data are normalized to  $^{134}\text{Ba}/^{136}\text{Ba}$ . Individual normalization factors were determined from the average of raw data of  $^{134}\text{Ba}/^{136}\text{Ba}$  ratios during the analyses, because  $^{134}\text{Ba}/^{136}\text{Ba}$  values of the uraninite samples are variable (see text).

$$\epsilon_{i\text{Ba}} = \left\{ \left( \frac{i\text{Ba}}{^{136}\text{Ba}} \right)_{\text{sample}} / \left( \frac{i\text{Ba}}{^{136}\text{Ba}} \right)_{\text{standard}} - 1 \right\} \times 10^4$$

Uncertainties are  $2\sigma$  of the mean.

Table 2. Fissiogenic Ba isotopic ratios

(a) clay

sample		$^{137}\text{Ba}_f/^{135}\text{Ba}_f$	$^{138}\text{Ba}_f/^{135}\text{Ba}_f$
BAX1190	#1	N.D.	N.D.
	#2	N.D.	N.D.
	#3	N.D.	N.D.
	#4	N.D.	N.D.
D75-5	#1	$0.57 \pm 0.25$	N.D.
	#2	N.D.	N.D.
	#3	$0.95 \pm 0.14$	N.D.
	#4	$0.56 \pm 0.24$	N.D.
D75-10	#1	$0.88 \pm 0.27$	N.D.
	#2	$0.54 \pm 0.24$	N.D.
	#3	N.D.	N.D.
	#4	N.D.	N.D.
D75-23	#1	N.D.	N.D.
	#2	N.D.	N.D.
	#3	N.D.	N.D.
	#4	$1.12 \pm 0.20$	N.D.
PX8-03	#1	$1.06 \pm 0.33$	N.D.
	#2	$1.30 \pm 0.39$	N.D.
	#3	$1.78 \pm 0.52$	N.D.
	#4	$1.89 \pm 0.40$	N.D.
PX8-9491	#1	$1.01 \pm 0.21$	N.D.
	#2	N.D.	N.D.
	#3	N.D.	N.D.
	#4	$1.014 \pm 0.003$	$1.355 \pm 0.025$
PX8-9794	#1	N.D.	N.D.
	#2	N.D.	N.D.
	#3	N.D.	N.D.
	#4	N.D.	N.D.

(b) uraninite

sample	$^{137}\text{Ba}_f/^{135}\text{Ba}_f$	$^{138}\text{Ba}_f/^{135}\text{Ba}_f$
SF84-1469		
#1	1.015 ± 0.010	1.475 ± 0.096
#2	1.013 ± 0.005	1.374 ± 0.047
#3	1.038 ± 0.007	1.607 ± 0.066
#4	1.054 ± 0.001	1.625 ± 0.001
SF84-1480		
#1	1.040 ± 0.005	1.624 ± 0.047
#2	1.049 ± 0.001	1.662 ± 0.005
#3	1.087 ± 0.001	1.804 ± 0.001
#4	1.086 ± 0.001	1.817 ± 0.001
SF84-1485		
#1	1.022 ± 0.001	1.592 ± 0.011
#2	1.027 ± 0.001	1.600 ± 0.008
#3	1.040 ± 0.001	1.650 ± 0.003
#4	1.180 ± 0.001	1.920 ± 0.001
SF84-1492		
#1	1.031 ± 0.001	1.566 ± 0.007
#2	1.029 ± 0.001	1.517 ± 0.009
#3	1.028 ± 0.001	1.556 ± 0.009
#4	1.182 ± 0.001	1.864 ± 0.001
D81N 260392		
#1	0.95 ± 0.19	N.D.
#2	1.626 ± 0.325	8.94 ± 2.84
#3	0.797 ± 0.170	N.D.
#4	1.116 ± 0.007	1.667 ± 0.061
SD37 S2/CD		
#1	N.D.	N.D.
#2	1.072 ± 0.016	2.055 ± 0.146
#3	1.058 ± 0.015	1.619 ± 0.131
#4	1.047 ± 0.006	1.538 ± 0.043

Table 3. Cs and Ba concentrations (ppm) in individual leachates from (a) clay and (b) uraninite samples

(a) clay				
sample		Cs	Ba	Cs/Ba
BAX1190				
	#1	0.284 ± 0.012	3.74 ± 0.06	0.0761 ± 0.0034
	#2	0.560 ± 0.014	29.5 ± 0.6	0.0190 ± 0.0006
	#3	0.829 ± 0.012	13.5 ± 0.4	0.0613 ± 0.0022
	#4	0.680 ± 0.018	10.6 ± 0.3	0.0644 ± 0.0025
D75-5				
	#1	0.176 ± 0.004	37.9 ± 1.1	0.00463 ± 0.00017
	#2	0.894 ± 0.028	343 ± 6	0.00261 ± 0.00009
	#3	1.92 ± 0.14	158 ± 14	0.0120 ± 0.0014
	#4	3.09 ± 0.06	32.7 ± 0.4	0.0944 ± 0.0022
D75-10				
	#1	0.136 ± 0.004	12.7 ± 0.4	0.0107 ± 0.0005
	#2	0.514 ± 0.008	192 ± 5	0.00268 ± 0.00008
	#3	1.70 ± 0.02	354 ± 10	0.00482 ± 0.00015
	#4	1.99 ± 0.08	65.2 ± 1.9	0.0306 ± 0.0015
D75-23				
	#1	0.113 ± 0.003	18.9 ± 0.2	0.00596 ± 0.00018
	#2	0.428 ± 0.010	157 ± 2	0.00271 ± 0.00007
	#3	1.89 ± 0.05	126 ± 3	0.0150 ± 0.0005
	#4	4.11 ± 0.08	22.8 ± 0.3	0.180 ± 0.004
PX8-03				
	#1	0.084 ± 0.001	7.92 ± 0.17	0.0106 ± 0.0002
	#2	0.275 ± 0.007	105 ± 1	0.00263 ± 0.00007
	#3	0.583 ± 0.013	198 ± 4	0.00295 ± 0.00009
	#4	0.670 ± 0.023	59.0 ± 2.0	0.0113 ± 0.0006
PX8-9491				
	#1	0.093 ± 0.001	21.1 ± 0.5	0.00442 ± 0.00011
	#2	0.645 ± 0.018	165 ± 1	0.00390 ± 0.00011
	#3	1.37 ± 0.05	195 ± 6	0.00703 ± 0.00032
	#4	4.58 ± 0.27	507 ± 32	0.00903 ± 0.00078
PX8-9794				
	#1	0.055 ± 0.002	28.1 ± 0.2	0.00197 ± 0.00007
	#2	0.442 ± 0.010	300 ± 5	0.00147 ± 0.00004
	#3	1.35 ± 0.04	78.7 ± 1.3	0.0171 ± 0.0005
	#4	2.97 ± 0.12	33.1 ± 0.9	0.0897 ± 0.0045



(b) uraninite

sample		Cs	Ba	Cs/Ba
SF84-1469				
	#1	0.061 ± 0.002	80.1 ± 1.8	0.00076 ± 0.00003
	#2	0.362 ± 0.003	83.8 ± 0.5	0.00432 ± 0.00005
	#3	0.621 ± 0.003	23.1 ± 0.1	0.0269 ± 0.0002
	#4	3.06 ± 0.04	101 ± 1	0.0303 ± 0.0006
SF84-1480				
	#1	0.152 ± 0.003	74.0 ± 1.6	0.00205 ± 0.00006
	#2	0.505 ± 0.004	61.4 ± 0.7	0.00822 ± 0.00011
	#3	1.92 ± 0.01	26.1 ± 0.2	0.0737 ± 0.0006
	#4	0.853 ± 0.015	12.1 ± 0.2	0.0707 ± 0.0015
SF84-1485				
	#1	0.121 ± 0.003	30.1 ± 0.8	0.00403 ± 0.00014
	#2	0.364 ± 0.021	70.4 ± 9.7	0.00518 ± 0.00078
	#3	0.816 ± 0.010	27.9 ± 0.2	0.0292 ± 0.0004
	#4	5.48 ± 0.08	64.2 ± 1.3	0.0855 ± 0.0021
SF84-1492				
	#1	0.114 ± 0.003	20.4 ± 0.2	0.00557 ± 0.00018
	#2	0.517 ± 0.002	160 ± 3	0.00323 ± 0.00006
	#3	0.791 ± 0.012	90.7 ± 1.2	0.00873 ± 0.00018
	#4	10.8 ± 0.1	103 ± 1	0.106 ± 0.001
D81N 260392				
	#1	0.066 ± 0.005	68.9 ± 4.5	0.00096 ± 0.00009
	#2	0.272 ± 0.007	470 ± 0.2	0.00058 ± 0.00001
	#3	0.432 ± 0.008	136 ± 2	0.00317 ± 0.00008
	#4	0.408 ± 0.010	59.3 ± 1.2	0.00687 ± 0.00022
SD37 S2/CD				
	#1	0.409 ± 0.012	50.5 ± 0.7	0.00809 ± 0.00027
	#2	1.25 ± 0.08	53.0 ± 3.0	0.0236 ± 0.0020
	#3	1.26 ± 0.04	11.0 ± 0.2	0.114 ± 0.004
	#4	0.882 ± 0.018	35.2 ± 1.0	0.0251 ± 0.0009

Table 4. Proportion of fissiogenic and non-fissiogenic Ba of RZ samples

sample	proportion (%)		concentration (ppm)	
	non-fissiogenic	fissiogenic	non-fissiogenic	fissiogenic
SF84-1469				
#1	99.82	0.18	79.95	0.147
#2	99.83	0.17	83.66	0.145
#3	99.83	0.17	23.06	0.038
#4	89.86	10.14	90.76	10.23
SF84-1480				
#1	99.77	0.23	73.83	0.170
#2	98.70	1.30	60.60	0.796
#3	86.38	13.62	22.55	3.55
#4	87.47	12.53	10.58	1.516
SF84-1485				
#1	99.45	0.55	29.93	0.167
#2	99.11	0.89	69.78	0.624
#3	97.14	2.86	27.10	0.798
#4	60.74	39.26	38.99	25.21
SF84-1492				
#1	98.53	1.47	20.10	0.299
#2	98.99	1.01	158.4	1.62
#3	99.20	0.80	89.98	0.722
#4	56.90	43.10	58.61	44.39
D81N 260392				
#1	99.99	0.01	68.90	0.005
#2	99.99	0.01	469.9	0.05
#3	99.99	0.01	135.99	0.011
#4	99.89	0.11	59.24	0.063
SD37 S2/CD				
#1	99.99	0.01	50.50	0.003
#2	99.94	0.06	52.97	0.033
#3	99.94	0.06	10.99	0.006
#4	99.85	0.15	35.15	0.054

Fig. 1 Hidaka and Gauthier-Lafaye

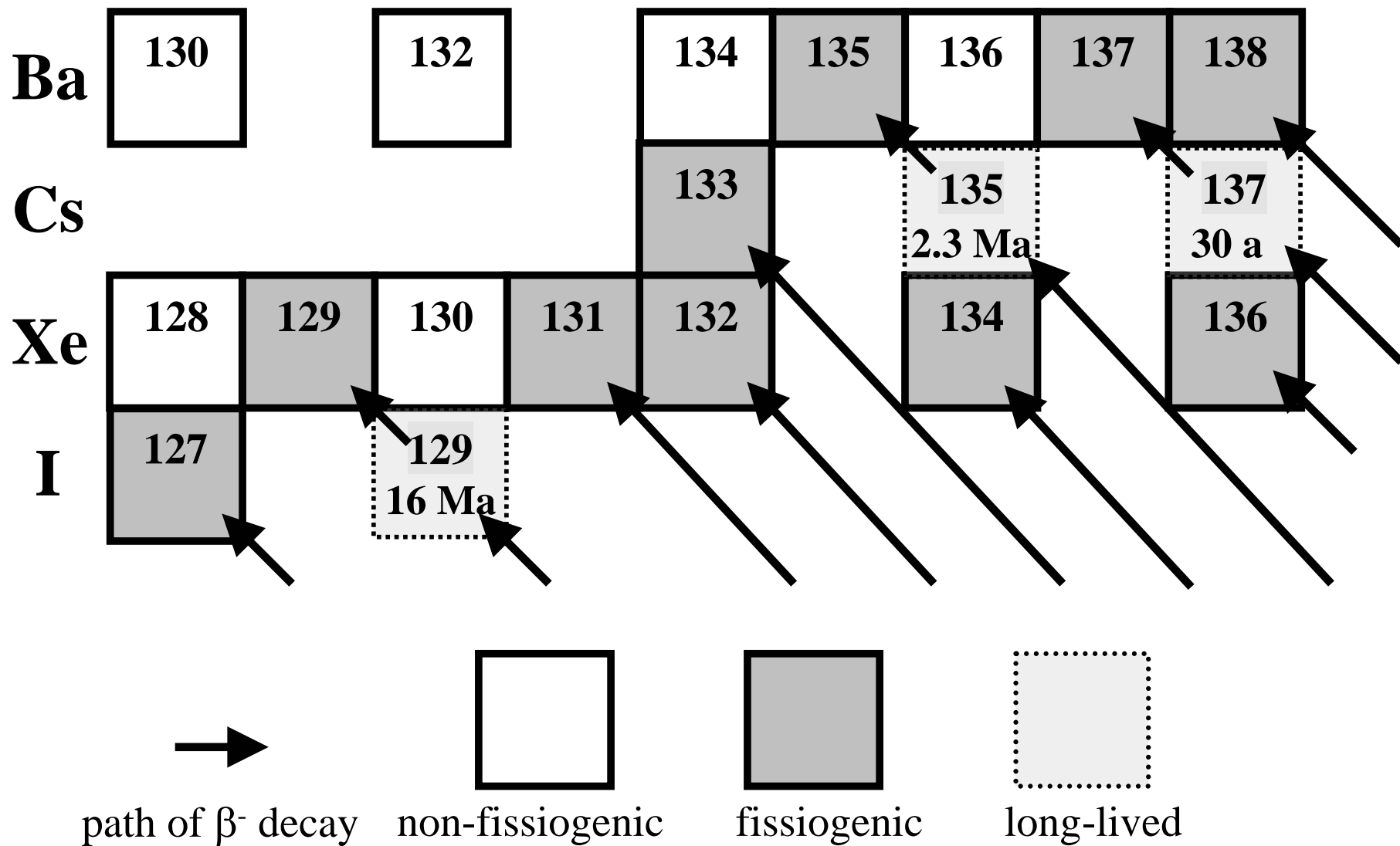


Fig. 2(A) Hidaka and Gauthier-Lafaye

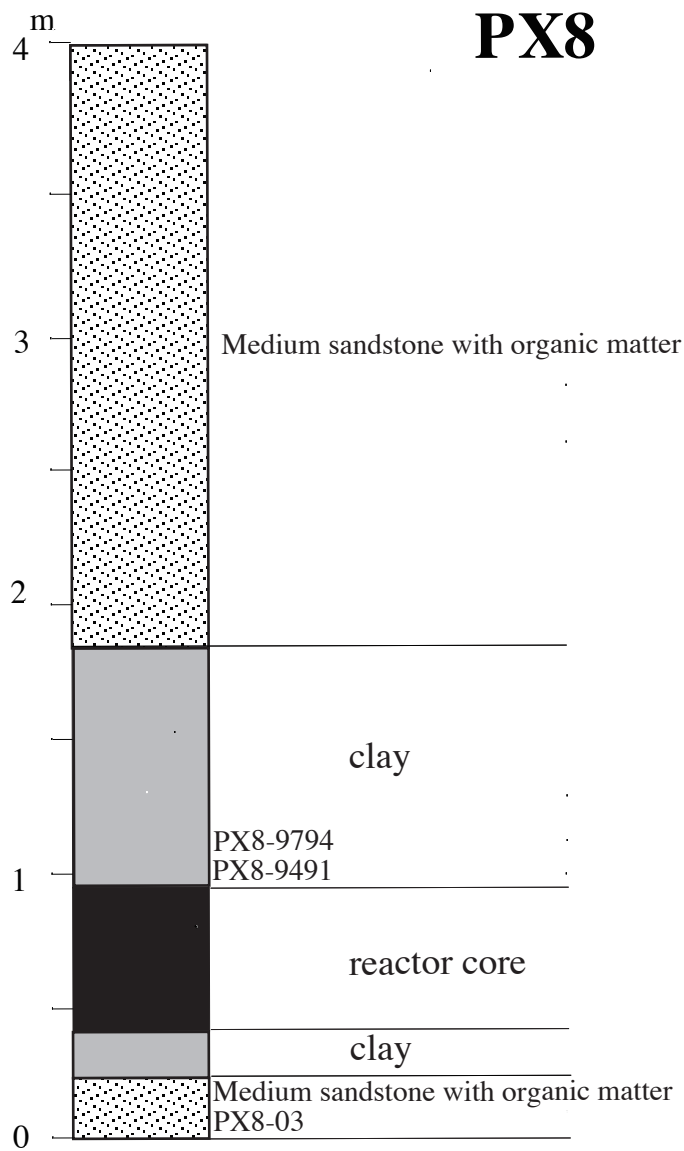
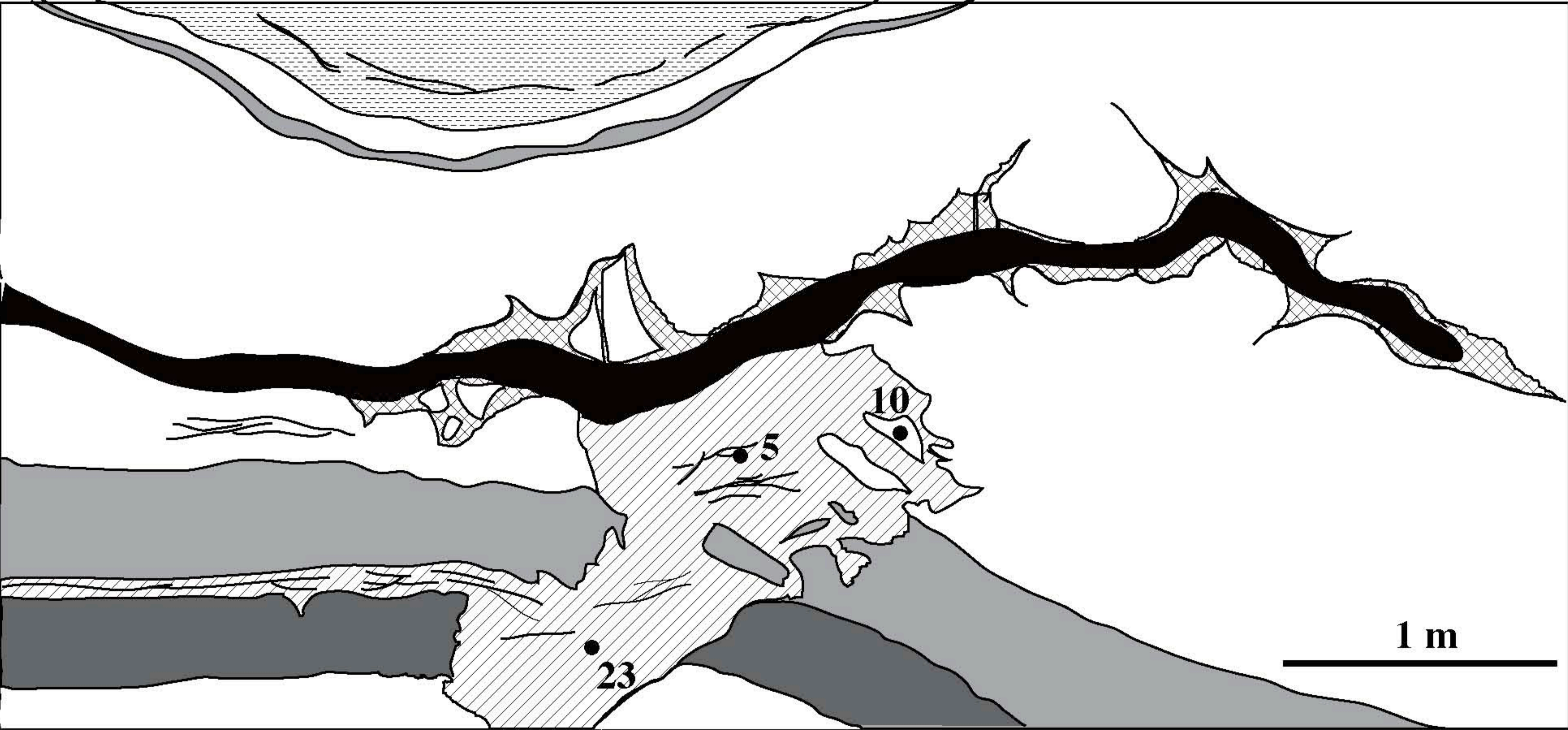




Fig. 2(B) Hidaka and Gauthier-Lafaye








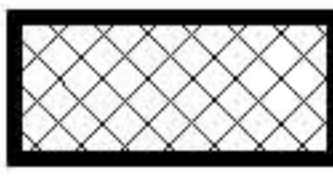


- |   |  |   |   |
|---|--|---|---|
|  sandstone |  fine sandstone |  clay        |  conglomerate      |
|  uraninite |  organic matter |  black shale |  sampling location |



Fig. 2(C) Hidaka and Gauthier-Lafaye

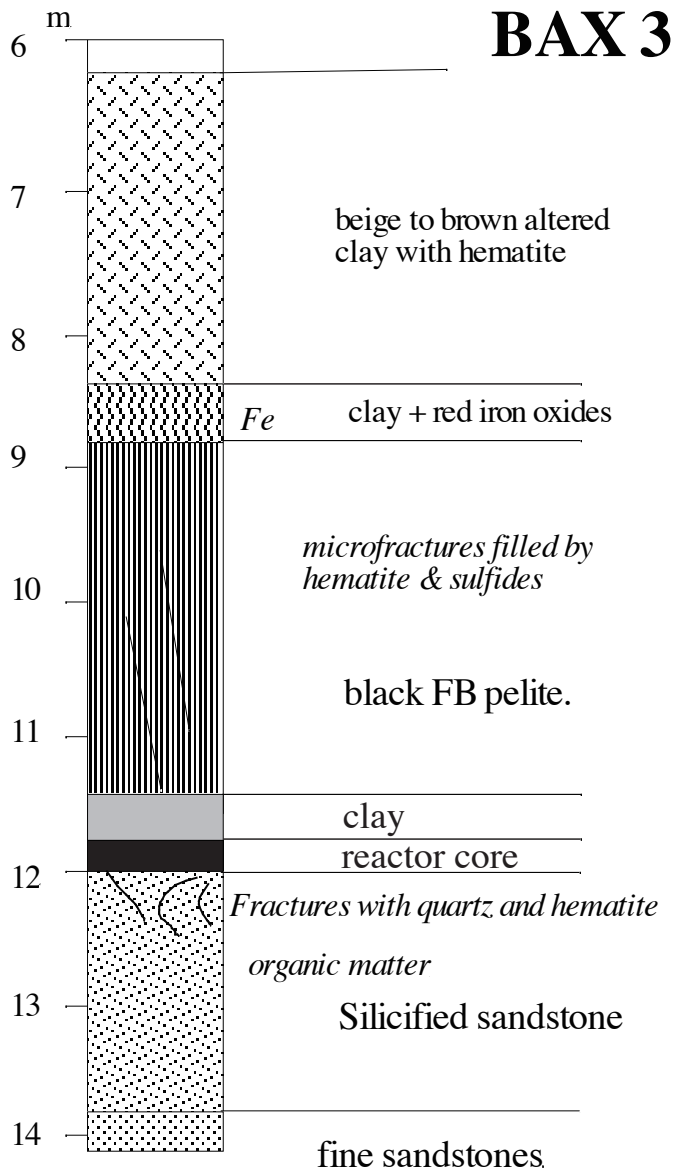


Fig. 3 Hidaka and Gauthier-Lafaye

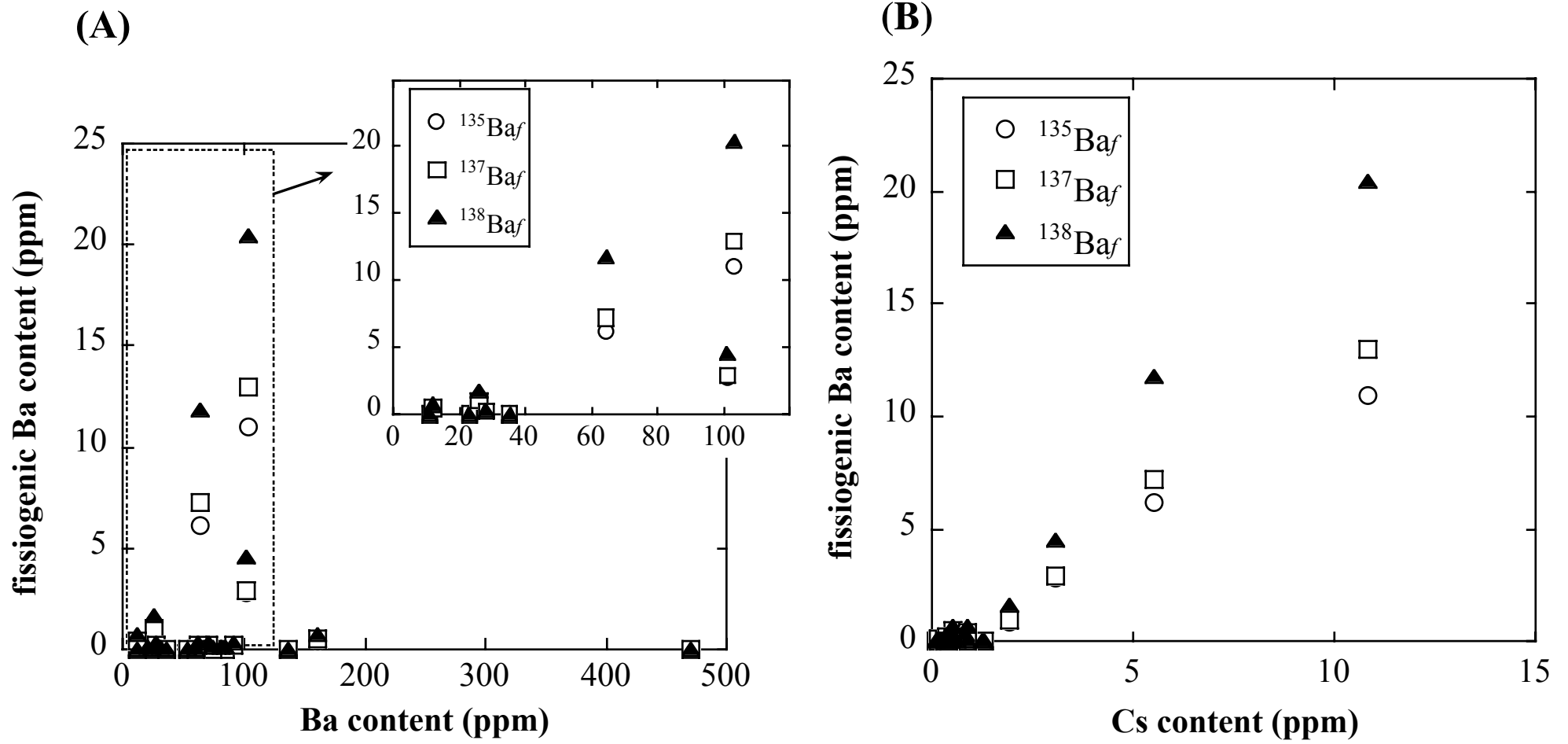


Fig. 4 Hidaka and Gauthier-Lafaye

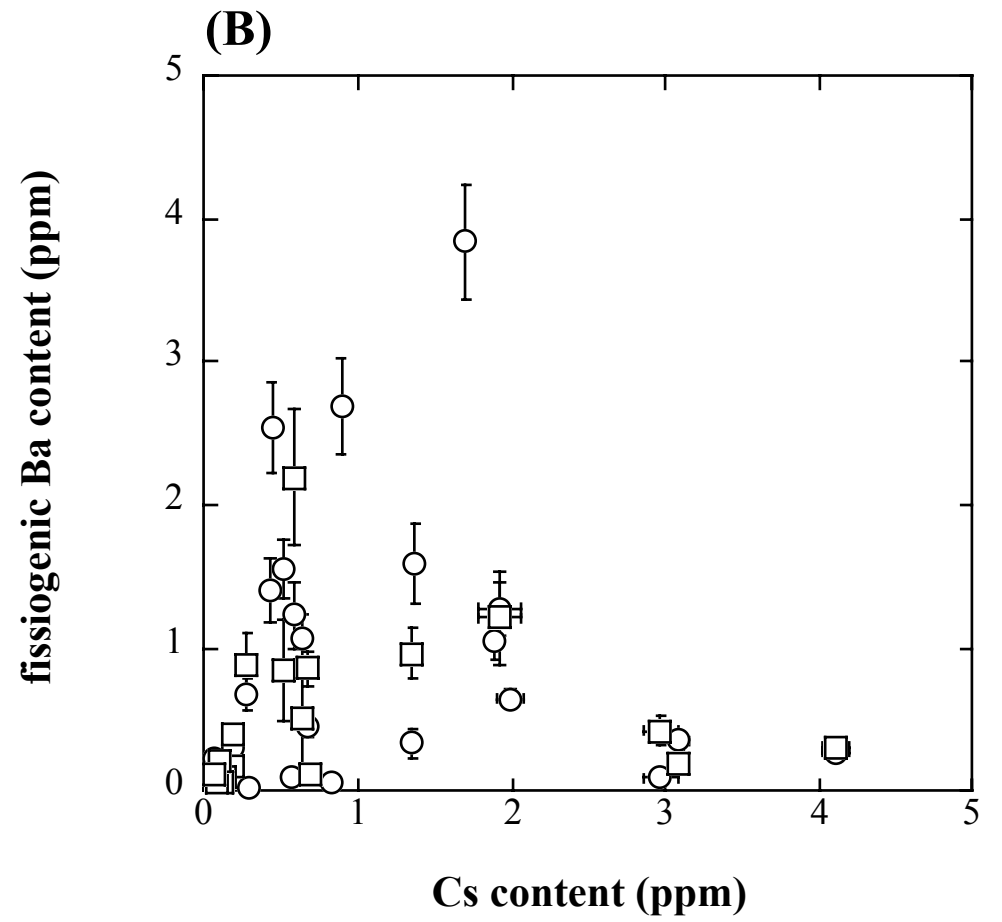
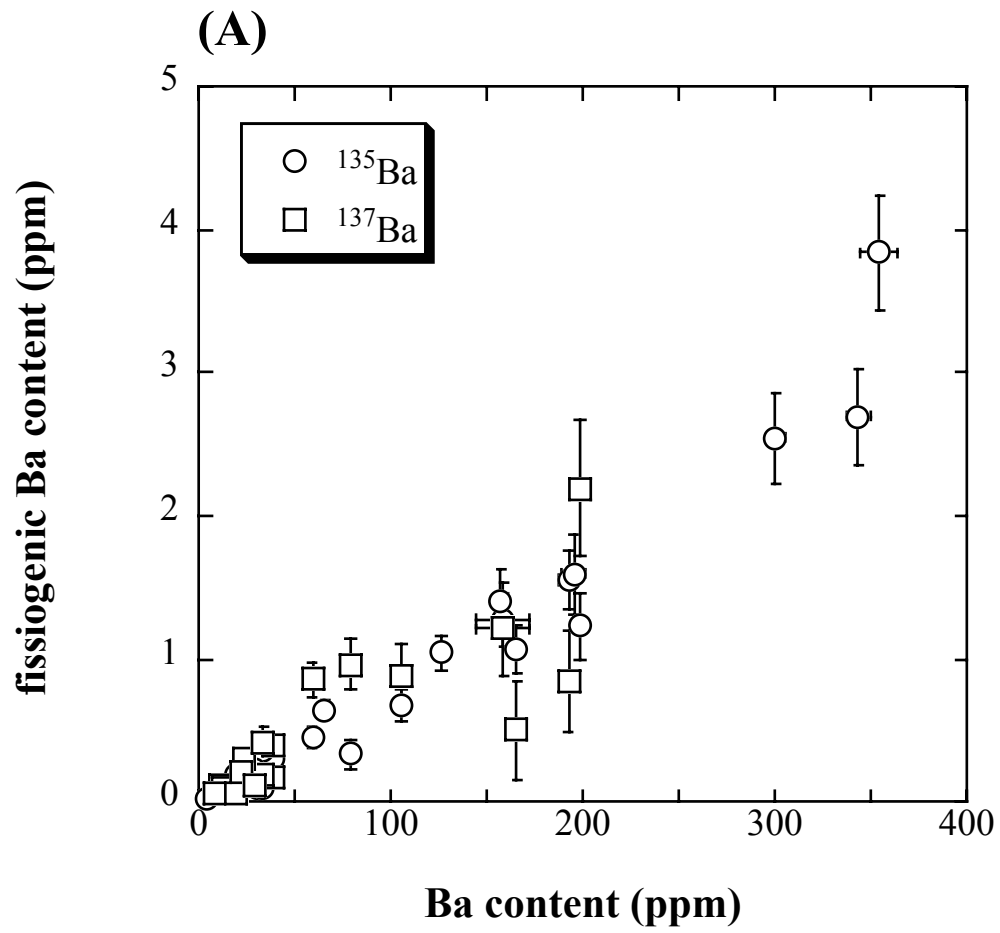




Fig. 5 Hidaka and Gauthier-Lafaye

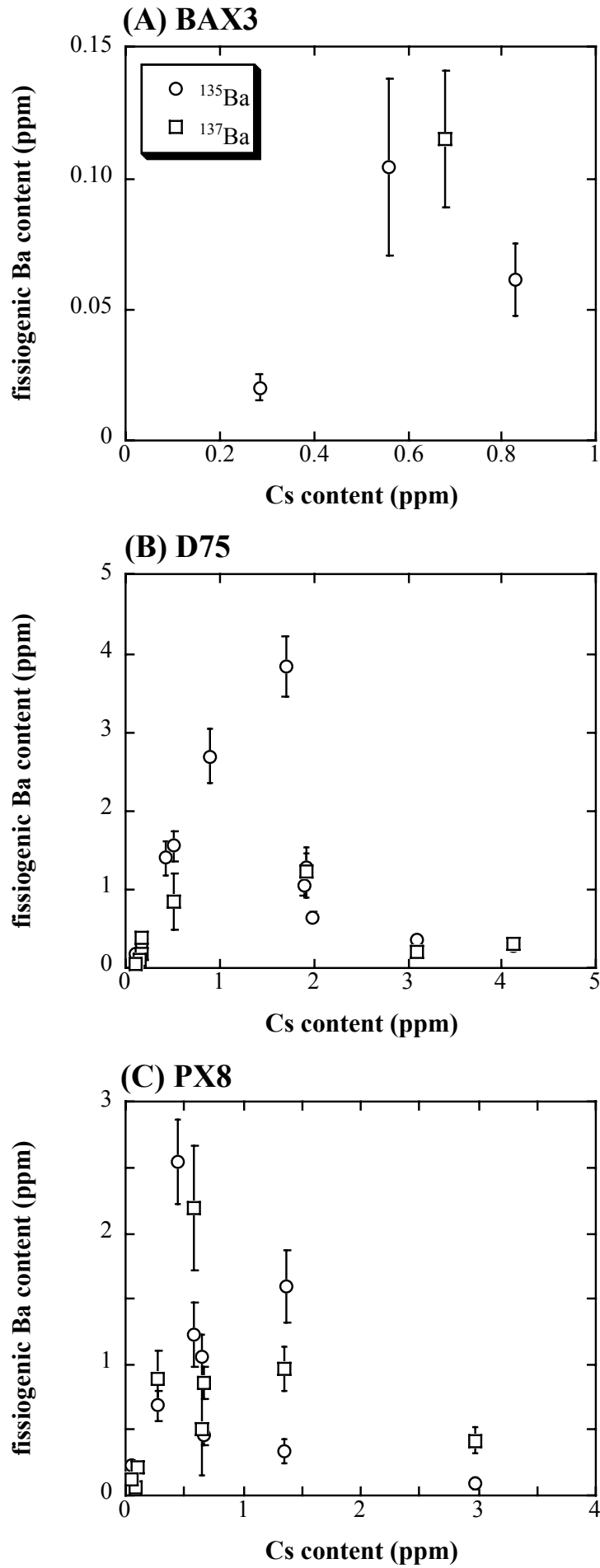


Fig. 6 Hidaka and Gauthier-Lafaye

